



## Comparative irradiation response of an austenitic stainless steel with its high-entropy alloy counterpart

M.A. Tunes<sup>a,b,1,\*</sup>, G. Greaves<sup>b</sup>, H. Bei<sup>c</sup>, P.D. Edmondson<sup>c</sup>, Y. Zhang<sup>c,d</sup>, S.E. Donnelly<sup>b</sup>, C. G. Schön<sup>e</sup>

<sup>a</sup> Chair of Non-Ferrous Metallurgy, Montanuniversitaet Leoben, Austria

<sup>b</sup> School of Computing and Engineering, University of Huddersfield, United Kingdom

<sup>c</sup> Materials Science and Technology Division, Oak Ridge National Laboratory, United States of America

<sup>d</sup> Department of Nuclear Engineering, University of Tennessee, United States of America

<sup>e</sup> Department of Metallurgical and Materials Engineering, Escola Politécnica da Universidade de São Paulo, Brazil

### ARTICLE INFO

#### Keywords:

High-entropy alloys  
Irradiation effects  
Microstructure  
Electron microscopy  
Transmission  
Energy systems

### ABSTRACT

Two metallic alloys in the quaternary system Fe–Cr–Mn–Ni were irradiated *in situ* within a transmission electron microscope (TEM) using Xe<sup>+</sup> heavy ions in the temperature range of 293–873 K and in the regime of low- (30 keV) and medium-energies (300 keV) with respective maximum doses of around 40 and 140 dpa. The first alloy is the FeCrMnNi high-entropy alloy (HEA) synthesised with the alloying elements close to equimolar composition. The second alloy is a commercial austenitic stainless steel AISI-348 (70.5Fe-17.5Cr-1.8Mn-9.5Ni wt.%), selected as the “low-entropy” counterpart of the FeCrMnNi HEA. Microstructural characterisation was carried out in the TEM with *in situ* heavy ion irradiation to investigate the role of entropy on radiation induced segregation and precipitation (RIS and RIP). The results demonstrated that among all the irradiation cases investigated, the FeCrMnNi HEA had its random solid solution matrix phase preserved in 80% of the experiments whilst the austenite matrix of the AISI-348 steel underwent RIP in 80% of the cases. It is therefore demonstrated that small differences between two alloys can lead to different radiation responses, confirming the trend that, by tuning the elemental composition superior radiation resistance can be achieved in metallic alloy systems, but emphasising that some of the constitutive core-effects of HEAs are still in need of further confirmation especially when the application of HEAs in energetic particle irradiation environments is considered.

### 1. Introduction

The evolution of physical metallurgy as the main branch of science addressing the relationship between microstructure, properties and processing of metals and alloys (and later of materials science, addressing all classes of materials) has brought – over the past century – unprecedented advances in several fields of human technology. Lightweight Al-, Mg- and Ti-based alloys entirely revolutionised modern industry with applications ranging from recyclable and high strength-to-weight ratio parts for both automotive and aerospace industries to the infant industry of biocompatible and biodegradable implants [1–13]. Fe-based alloys – in particular steels – have formed the backbone of our technology thus far [14,15] and are still just as relevant in modern technology as structural materials. The combination of metallic alloys

such as steels with Zr-based alloys has led to the success of both thermal- and fast-neutron reactors [16–18], providing clean electricity making up 10% of the world’s energy supply [19].

Throughout history, the great majority of metallic alloys were developed based on available raw materials [20–22]. The occurrences of such raw materials, in most cases, consist of minerals of a given element and require particular technologies to be exploited. This led to the development of specific metal industries, each one characterized by its own knowledge set. Traditionally, alloys developed within one of these sets were named after the particular metal, so, the Cu industry developed Cu alloys, the Fe industry developed steels and cast irons, the Al industry develops Al alloys, and so on. Naturally in most cases that particular metal is predominant in the alloy, but not necessarily.

This resulted in the notion of the terminal solid solution principle

\* Corresponding author. Chair of Non-Ferrous Metallurgy, Montanuniversitaet Leoben, Austria.

E-mail addresses: [tunes@lanl.gov](mailto:tunes@lanl.gov), [m.a.tunes@physics.org](mailto:m.a.tunes@physics.org) (M.A. Tunes).

<sup>1</sup> Present address: Materials Science and Technology Division, Los Alamos National Laboratory, United States of America.

which would consist of alloying a base metal with a small content of either major or minor solutes, which today are supposedly selected following the formalisation of the Hume-Rothery rules [23,24], but in fact empirical experience is often used. Using the perspective of the thermodynamics of alloy systems, terminal solid solution alloys (sometimes referred to as dilute alloys) are those engineered considering the solute-rich corner of phase diagrams [24]. Naturally this is a gross simplification of the technical alloys' universe and there are plenty of examples which are neither based on the terminal solid solution (e.g. the so called beta bronzes), nor can be described as dilute alloys (e.g. stainless steels).

Most recently, the science of metallurgy has been impacted with the advent of a new class of metallic alloys: the high-entropy alloys (or HEAs) [25]. As opposed to terminal solid solutions, HEAs are metallic alloys designed at or closer to the highly concentrated centre of phase diagrams. Although HEAs attracted the attention of the materials science and metallurgy communities only in the past 15 years, the idea of casting highly concentrated alloys is far from new; in fact, it dates back to the eighteenth century. In 1778, Achard reported [26] his discoveries after casting and characterising around 1000 metallic alloys with Ag, Pt, Co, Cu, Fe, Pb, Sn, Zn, Bi, Sb and As. According to Murty et al. [25], Achard was probably the first metallurgist to synthesise equiatomic multicomponent alloys. His work was revisited two centuries later by the research groups of Cantor and Yeh working independently with focus on the quinary equiatomic alloy FeCrMnNiCo [25,27–34].

The distinct properties of HEAs compared with conventional diluted alloys were reviewed recently by Murty et al. [25]. It is believed that alloying in the highly-concentrated region of the multicomponent metallic systems results in a strong thermodynamic stabilisation of a single-phase structure with a random site-occupancy for substitutional solutes: this is an important core-effect of HEAs known as the "high-entropy effect" [33]. At the foundation of this core-effect lies the hypothesis that the Boltzmann configurational entropy [35–37] – as shown in equation (1) – dominates the entropic contribution in promoting the thermodynamic stabilisation as an equiatomic alloy composition (the composition of each *i*-th constituent of the alloy is denoted as  $x_i$  in equation (1)) will maximises the whole entropy of the system, thus reducing its Gibbs free energy even at high temperatures [25,27–34].

$$\Delta S_{conf} = -k_B N_A \sum_{i=1}^N x_i \ln x_i \quad (1)$$

Severe lattice distortion and sluggish diffusion are two important core-effects of HEAs recently under intense research. The first occurs as a direct consequence of the random solid solution principle which generates a distorted crystal structure as each lattice equilibrium position has an element with different atomic radius. The second core-effect (hypothesised by Yeh et al. [38] and Chang et al. [39]) suggests that solid-state diffusion and phase transformation kinetics are both suppressed and/or retarded in HEAs when compared with diluted solid solution alloys. The "sluggish" solid-state diffusion in HEAs would presumably occur due to the large fluctuation of the lattice potential energy and high activation energy barriers, both closely related to the local chemical environment [25,40–43]. Experiments recently indicated that the sluggish diffusion core-effect might affect several synthesis and processing parameters in HEAs, for example nucleation and growth of precipitates, reduced grain coarsening rate and increased creep resistance [25].

Both high-entropy and sluggish diffusion core-effects are of interest to the nuclear materials community as a (more) thermodynamically stable material with suppressed diffusion of point defects induced by irradiation would result in an alloy with superior radiation tolerance when compared with the conventional diluted alloys often used in nuclear materials such as Fe- and Zr-based alloys. In fact, several scientists have already reported that HEAs are of superior radiation resistance [44–55]. Despite such reported stability under irradiation, some

questions remain to be answered: are these constitutive HEA core-effects real? Is the configurational entropy behind the single-phase random solid solution stabilisation and sluggish diffusion, thus leading to radiation tolerance? In fact, criticism of the constitutive hypotheses of the HEAs was presented by Bhadeshia in an editorial article in 2015 [56]. Four critical points were raised by Bhadeshia regarding the emerging concept of HEAs and are summarised below:

1. The concept of ideal solid solutions has been used to shed light on the core-effects of HEAs although ideal solid solutions simply do not exist;
2. The dominance of the configurational entropy factor in the Gibbs free energy assumes that the enthalpy of mixing in a HEA is negligible. But as the HEAs should not be considered ideal solid solutions, the quasi-chemical approach [57,58] should be used instead where the enthalpy is not (always) negligible;
3. HEAs are in fact already satisfying existing metallurgical principles and they should not be considered different than conventional dilute alloys. For example, the addition of Cr to equimolar concentrations results in increased corrosion resistance simply because Cr itself improves corrosion resistance [59] (unless precipitation is favoured in a certain metallic system);
4. Regarding the mechanical properties, it is often mentioned [60] that the atomic misfit causing lattice strain would restrict the motion of dislocations, resulting in unique mechanical strength for HEAs. But the concept of lattice strain induced by atomic misfit is not clear considering that in an HEA the distinction between solute and solvent does not exist.

Along with Bhadeshia [56], recent criticism of both sluggish diffusion [42,61–63] and high-entropy core-effects [64–66] indicate that the constitutive hypothesis of HEAs is still awaiting a more definitive confirmation, especially whether they are attributed as the main reason for such a superior resistance to energetic particle irradiation. In this present paper, we target the hypothesis of configurational entropy behind higher alloy thermodynamic stability, thus high radiation resistance. Heavy ion irradiation *in situ* within a Transmission Electron Microscope (TEM) is used for real-time monitoring of the effects of irradiation in two similar alloys, the austenitic stainless steel grade 348 (71.2Fe-17.5Cr-1.8Mn-9.5Ni wt.%) as a "low-entropy" alloy and its equivalent high-entropy alloy (26.8Fe-18.4Cr-27.3Mn-27.5Ni wt.%). In order to compare the response to irradiation in both alloys, the microstructural characterisation within the TEM was focused on analysing any defects in the alloys under bright-field conditions and the stability of the matrix phases using selected-area electron diffraction.

## 2. Materials and methods

### 2.1. Alloys synthesis and processing

A plasma arc melting furnace and drop casting were used to synthesise the FeCrMnNi HEA bulk at the Oak Ridge National Laboratory and more specific details on the procedure have been published elsewhere [50]. The AISI-348 steel belongs to the 300-series of austenitic stainless steels and it was commercially obtained (AISI is the designation of the American Iron and Steel Institute). The grade 348 contains Nb as a minor solute and according to Padilha et al. [67] these austenitic stainless steels are often solution-annealed at temperatures around 1300 K and air-cooling is sufficient to warrant a cooling rate to avoid the sensitisation of the austenite matrix. Information of the complete thermo-mechanical processing of the AISI-348 steel used in this work was not provided by the distributor (FOPIL [68]) as it is considered proprietary information, but it presumably followed the usual metallurgical procedure, in which the alloy is continuously cast and sequentially rolled with multiple passes, while its temperature is decreasing, until the final state where a sheet is obtained. In their pristine condition,

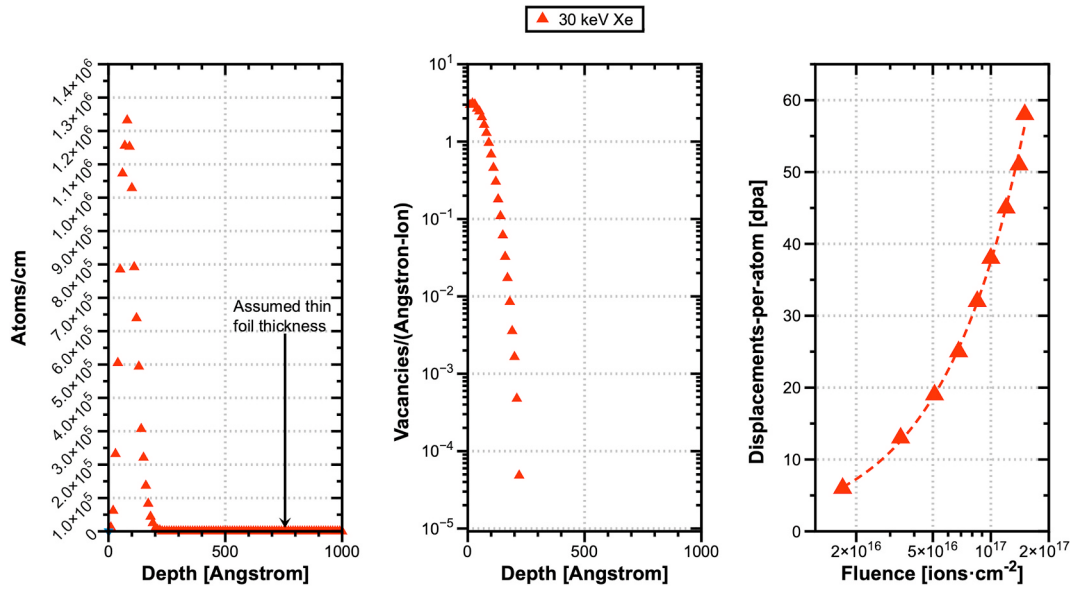


**Fig. 1.** SRIM-2013 implantation, damage and fluence-to-dpa profiles for 30 keV Xe irradiation in both FeCrMnNi HEA and AISI-348 steel.

both alloys are in the annealed state.

## 2.2. Electron-microscopy sample preparation

Due to limited material availability, electron-transparent lamellae from the FeCrMnNi HEA bulk were prepared using the lift-out technique [69] within a FEI Quanta 3D Scanning Electron Microscope (SEM) and Focused Ion Beam (FIB). For the AISI-348 steel, the technique of electro-chemical jet polishing (ECJP) was used to produce electron-transparent 3 mm discs using a 10% perchloric acid with 90% methanol solution at temperature of 233 K and an electric potential of 20 V. ECJP was performed until perforation of the 3 mm discs which were then left to dry in the air after several pure methanol washing baths. For clarification and comparison with the experiments performed with FeCrMnNi HEA, a limited number of electron-transparent lamellae of the AISI-348 steel were also produced using the lift-out FIB technique,

but it is worth emphasising that regardless of the sample preparation method, the results obtained with the AISI-348 steel were reproducible.

## 2.3. Pre- and post-irradiation characterisation

Extensive pre-irradiation characterisation was performed in both studied alloys with a combination of methods. For elemental composition estimation both inductively coupled plasma atomic emission spectroscopy (ICP-OES) and Energy Dispersive X-ray Spectroscopy (EDX) were used. In the case of the steel, the composition was furnished by the steel provider (as measured by ICP-OES) and it is found in Ref. [70]. Transmission Electron Microscopy (TEM) was carried out in both alloys following sample preparation: Bright-Field (BF), Dark-Field (DF) and Selected-Area Electron Diffraction (SAED) were used in this work. Under BF conditions, samples were also screened using defocusing phase contrast (also known as Fresnel contrast) in order to analyse the

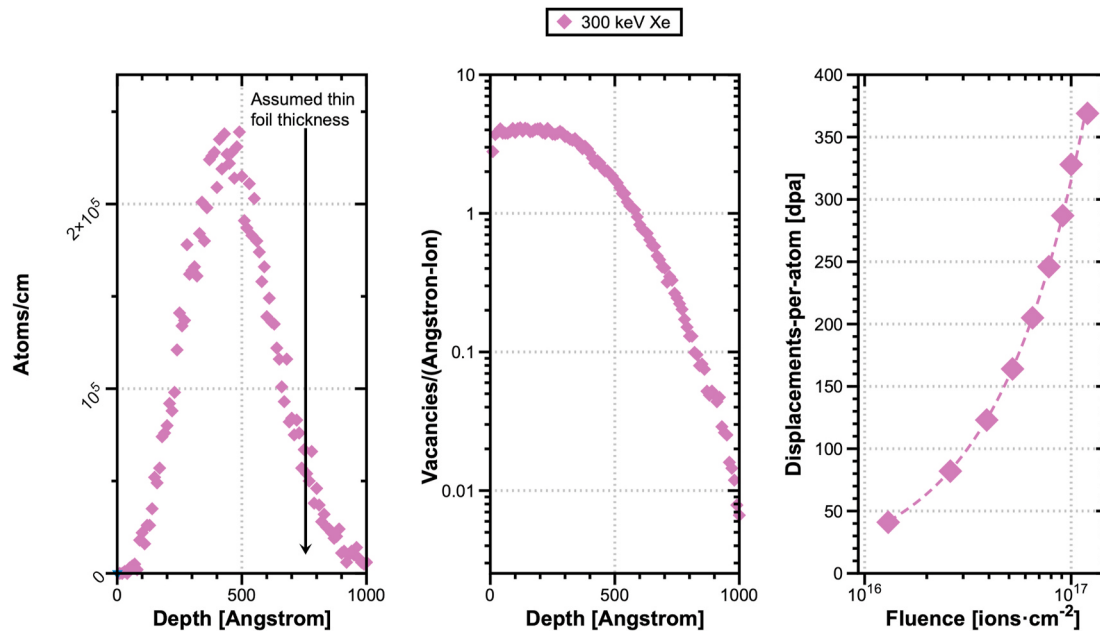
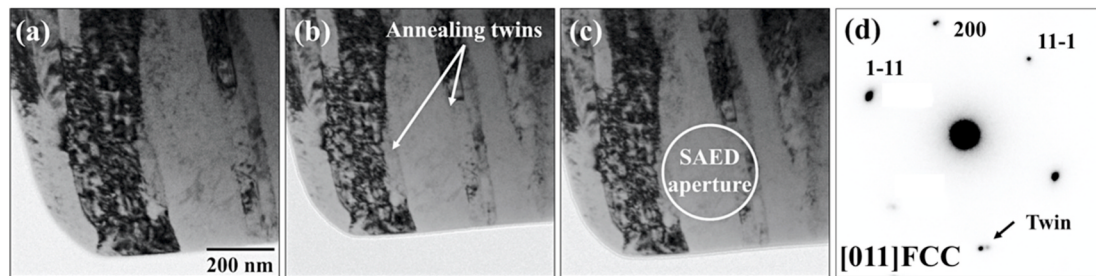


**Fig. 2.** SRIM-2013 implantation, damage and fluence-to-dpa profiles for 300 keV Xe irradiation in both FeCrMnNi HEA and AISI-348 steel.

## FeCrMnNi HEA



## AISI-348 steel

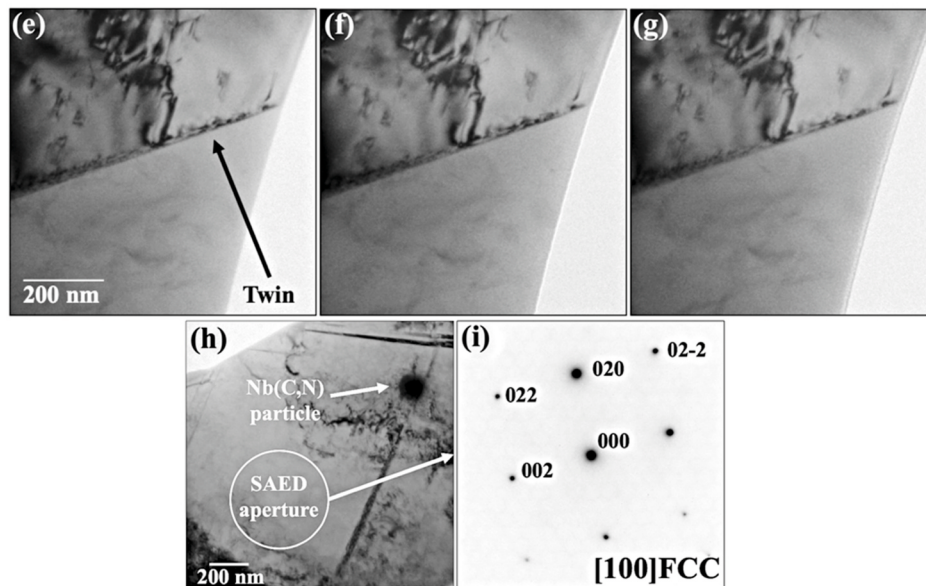


**Fig. 3.** Characterisation of the pristine alloys studied in this work. The BFTEM micrographs of the FeCrMnNi HEA are shown in micrographs (a–c) where (b) and (c) were taken under and overfocus (defocus of 800 nm). The BFTEM micrographs of the AISI-348 steel are shown in figures (e–h) where (f) and (g) were taken under and overfocus (defocus of 1000 nm). The micrographs (d) and (i) are SAED patterns recorded with the aperture positioned as indicated in (c) and (h), respectively. Note: the scale bar in (a) also applies to (b) and (c) and the scale bar in (e) also applies to (f) and (g).

presence of voids and inert gas bubbles before and after irradiation. SAED pattern indexing was carried out using reference data provided by Howe et al. [71], Rarey et al. [72] and verified again using an austenite (FCC) model in the software CrystalMaker/SingleCrystal with crystallographic data available from Oila et al. [73].

#### 2.4. Heavy ion irradiations *in situ* within a TEM and fluence-to-dpa conversion

Heavy ion irradiations *in situ* within a TEM were carried out using the MIAMI-2 system at the University of Huddersfield [74] using two energy configurations: 30 keV (low-energy) and 300 keV (medium-energy) Xe ions. Both FeCrMnNi HEA and AISI-348 steel were subjected to irradiations up to the same doses. For 30 keV Xe irradiations the flux (at the specimen position within the TEM) was around  $4.2 \times 10^{13}$  ions·cm $^{-2}$ ·2s $^{-1}$  whilst for 300 keV Xe irradiations the measured flux was around  $2.0 \times 10^{13}$  ions·cm $^{-2}$ ·2s $^{-1}$ . SRIM-2013 [75] was used to estimate the implantation and damage profiles for both irradiation conditions which are shown in Figs. 1 and 2, respectively.

Fluence-to-dpa conversion was performed with a procedure proposed by Stoller et al. [76] using the “quick calculation damage” option, although a recent work [77] has pointed out that the use of this procedure for estimating dpa in multi-elemental targets may lead to inaccurate fluence-to-dpa conversion results as the NRT model used in the

quick calculation option within SRIM-2013 lacks modern ion-solid interaction physics. Note that, throughout this present work, dpa values are given in the text, but the figures contain both fluence and dpa values for reference. The displacement energy for each of the constituents of both alloys (FeCrMnNi) was set to 40 eV in the SRIM code. The thickness of the specimens was around 70 nm as-measured using Electron Energy Loss Spectroscopy (EELS) and this value was used for the fluence-to-dpa conversion. Given the similarities between the studied alloys, their volumetric mass density ( $\approx 8.0$  g·cm $^{-3}$ ) and atomic density ( $8.7 \times 10^{22}$  atoms·cm $^{-3}$ ) were assumed to be the same for calculation purposes. Under 30 and 300 keV Xe irradiations, the number of displacements per ion collision in both alloys was estimated by SRIM to be 220 and 1900, respectively. For example, under such conditions a fluence of  $5.7 \times 10^{16}$  ions·cm $^{-2}$  corresponds to 21 dpa for 30 keV Xe ions whilst a fluence of  $4.4 \times 10^{16}$  ions·cm $^{-2}$  corresponds to 140 dpa for 300 keV Xe ions. Plots showing the complete scenario of fluence and dpa for low- and medium-energy irradiations are shown in Figs. 1 and 2, respectively.

## 3. Results and discussion

We report the results obtained with the pre-irradiation characterisation and the heavy ion irradiations *in situ* within a TEM of the two alloys investigated in this work: the AISI-348 steel and the FeCrMnNi

**Table 1**

The elemental composition of the FeCrMnNi HEA measured by SEM-EDX (the error is  $\pm 5\%$  for each value).

Element	Composition [wt.%]
Fe	26.8 $\pm$ 1.3
Cr	18.40 $\pm$ 0.9
Ni	27.50 $\pm$ 1.4
Mn	27.30 $\pm$ 1.4

**Table 2**

The elemental composition of the austenitic stainless steel AISI-348 measured by ICP-OES (the error is  $\pm 1\%$  for each value) (also reported previously in Ref. [70]).

Element	Composition [wt.%]
C	0.037
S	<0.001
P	0.002
Ni	9.47
Si	0.36
Mn	1.81
Cr	17.50
Co	<0.001
B	<0.008
Ta	0.003
Nb	0.32
Fe	70.48

HEA. Although a brief discussion on the results will be given in this section, a more comprehensive assessment of the radiation response of both alloys is in section 4. For each irradiation case investigated and for

each alloy studied, two (or more than two in some cases) independent experiments were carried out starting with pristine samples.

### 3.1. Pre-irradiation characterisation of the alloys

A pre-irradiation characterisation of the AISI-348 steel and the FeCrMnNi HEA before the irradiation is shown in Fig. 3. BFTEM micrographs of the pristine FeCrMnNi HEA are shown in Fig. 3(a–c) at focus, under and overfocus (defocus of 800 nm) conditions, respectively, and they show that the HEA has no voids or bubbles in its pristine condition. Similarly, BFTEM micrographs in Fig. 3(e–g) exhibit the pristine microstructure of the AISI-348 steel. No voids or bubbles were detected prior to irradiation as shown in the under and overfocus (defocus of 1000 nm) micrographs in Fig. 3(f) and (g), respectively. The SAED patterns for both alloys are shown in Fig. 3(d) and (i). These patterns were indexed to be of face-centred cubic (FCC) structure confirming previous reports on both alloys [44,50,62].

Two particular features distinguish the AISI-348 steel and the FeCrMnNi HEA from a microstructural perspective. Comparing the BFTEM micrographs in Fig. 3(a–c) with the micrographs in Fig. 3(e and f), one can notice that the FeCrMnNi HEA has a higher density of twins than the AISI-348 steel. At the same time, as a result of the addition of Nb, the AISI-348 steel has rounded nanoparticles of Nb(C,N) as dispersoids in its matrix phase. The first observation is that alloying within the centre of the phase diagrams decreases the stacking fault energy of certain metallic systems [78], thus allowing the nucleation and growth of large twins during processes such as solution heat-treatment and/or thermal annealing. In this way, the FeCrMnNi HEA is more prone to the nucleation and growth of annealing twins than the AISI-348 steel. With respect to the Nb(C,N) nanoparticles, this topic was extensively studied by Silcock et al. [79] who concluded that the continuous segregation of Nb and C into stacking faults within the austenite is a governing factor

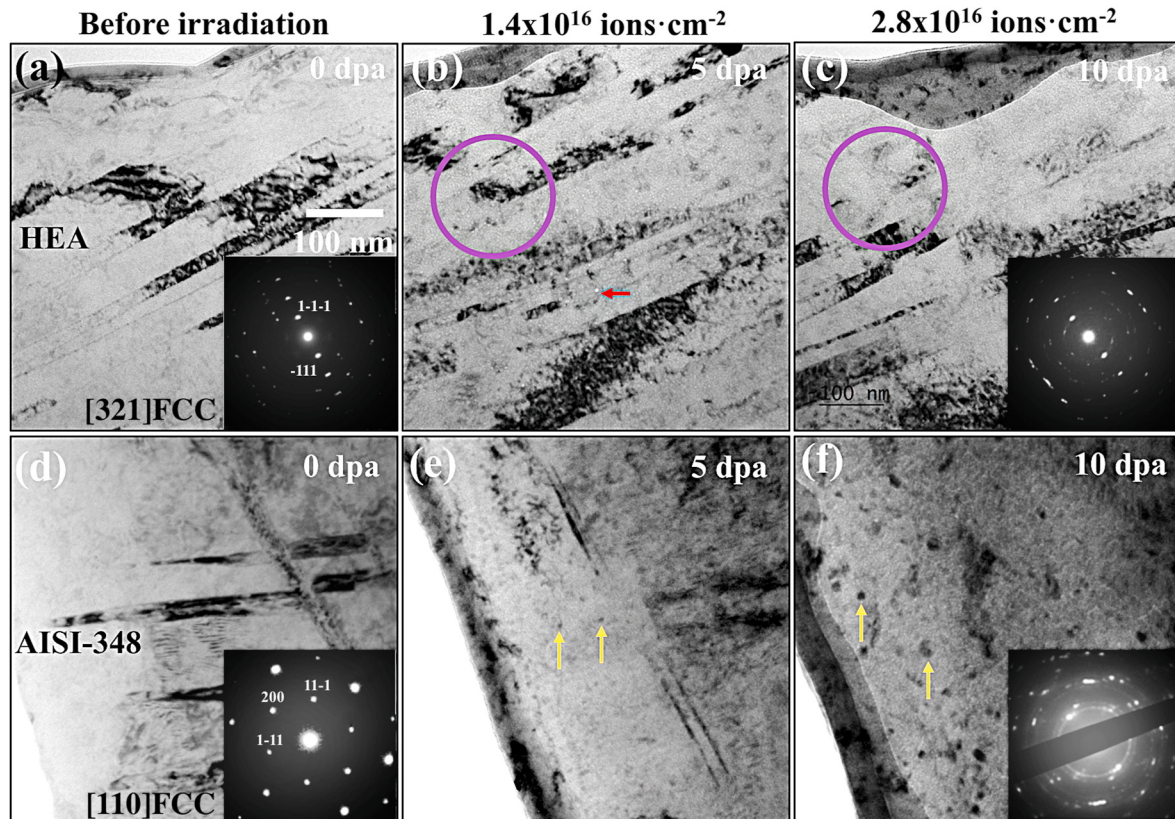


**Fig. 4.** Real-time response of the FeCrMnNi HEA (a–c) and the AISI-348 steel (d–f) upon low-energy heavy ion irradiation up to 10 dpa at 293 K. Note: the scale bar in (a) also applies to (b) and (c) and the scale bar in (d) also applies to (e) and (f).

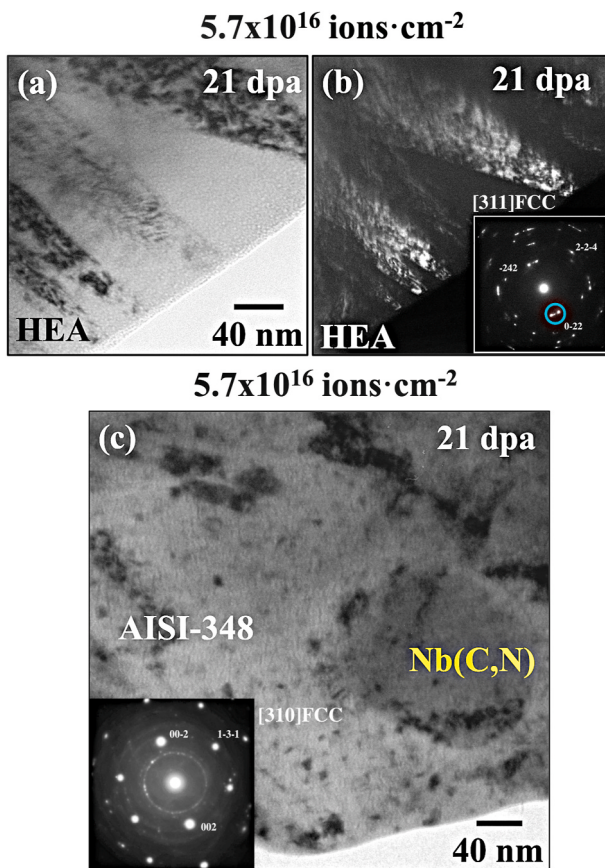


**Fig. 5.** Microstructures of the (a–b) FeCrMnNi HEA and the (c) AISI-348 steel after low-energy heavy ion irradiation up to 21 dpa at 293 K. Whilst the FeCrMnNi HEA preserves its random solid solution during irradiation, the austenite matrix of the AISI-348 steel is observed to decompose into nanometre-sized precipitates.

for the nucleation of rounded-shape Nb(C,N) precipitates. A detailed quantitative and qualitative characterisation of the Nb(C,N) precipitates in the austenite matrix of the AISI-348 steel in comparison with the relevant literature review [80] was recently performed by Tunes [81].

Still on twinning, as noted in Fig. 3(c), the SAED aperture only partially covers the twin on its right side, therefore, a single satellite spot (characteristic of twinning in austenitic stainless steels [82–87]) is seen in the diffraction pattern in 3(d). In addition, it is worth emphasising that for better visualization of radiation damage under BFTEM conditions, the micrographs were taken slightly off-zone axis which also impair a more detailed twin characterisation.

The pre-irradiation characterisation revealed that both alloys are of FCC structure, have twins in their matrix phase (with a higher density in the FeCrMnNi HEA) and the AISI-348 steel has Nb(C,N) precipitates in its austenite matrix. Analytical characterisation using ICP-OES and EDX revealed the elemental composition of both alloys as shown in Tables 1 and 2. Morphologically, the two alloys are of equiaxed grain structure and despite small differences such as the large annealing twins in the FeCrMnNi HEA and the Nb(C,N) precipitates in the AISI-348 steel, the two alloys studied in this work can be considered similar. Essentially, the major difference between the two alloys are in fact the elemental composition.

### 3.2. Low-energy heavy ion irradiation

Low-energy heavy ion irradiation has been carried out *in situ* within the TEM in the temperature range from 293 to 873 K and the results are shown in this section. As noted by English et al. [88], low-energy heavy

ion irradiation (typically  $E \leq 200$  keV up to fluences of around  $10^{13}$  ions·cm<sup>-2</sup>) is an interesting alternative to emulate the effects damage cascades generated by neutron irradiation in  $\alpha$ -Fe. Typical PKA average energies generated by fast neutrons in a common light-water reactor are  $\approx 10$  keV [89]. The PKA average energy of Fe when irradiated with 30 keV Xe ions is 11.7 keV as calculated with the SRIM code.

#### 3.2.1. 293 K

The real-time response to 30 keV Xe ions of both the FeCrMnNi HEA and the AISI-348 steel at 293 K up to 10 dpa is shown in Fig. 4(a–c) and Fig. 4(d–f), respectively. Xe bubbles were detected in the two alloys at 5 dpa. The austenite matrix phase of the AISI-348 steel was observed to decompose as monitored by the SAED patterns shown as insets of micrographs 4(d) and 4(f): the initial single crystal austenite at 0 dpa transformed into a microstructure full of small crystalline precipitates indicated by the yellow arrows in the BFTEM micrographs 4(e) and 4(f) as well as confirmed by the presence of Debye-Scherrer rings in the SAED pattern in 4(f). Similar radiation-induced precipitation (RIP) effects were not observed to occur in the FeCrMnNi HEA which remained fully crystalline without precipitates up to 10 dpa. Black-spots developed in the microstructure of the FeCrMnNi HEA at around 5 dpa (purple circles in Fig. 4(b) and (c)), but a trend for their annihilation upon increasing the dose was observed. The red arrow in micrograph 4 (b) also points to Xe bubbles growing with dose at 5 dpa, but at higher doses such large bubbles vanished, i.e. in the FeCrMnNi HEA there is a trend for annihilation of both black-spots and Xe bubbles.

The set of BFTEM and DFTEM micrographs in Fig. 5(a) and (b), respectively, shows that the FeCrMnNi HEA has Xe bubbles in its matrix phase at 21 dpa, but it remarkably exhibits no nanometre-sized precipitates as is the case for the AISI-348 steel. This is also confirmed by the SAED pattern inset in Fig. 5(b): apart from the satellite spots corresponding to pre-existing annealing twins, no Debye-Scherrer rings were detected in the FeCrMnNi HEA.

**3.2.2. 573 K.** The real-time response to low-energy heavy ion irradiations at 573 K is shown in Fig. 6(a–c) and 6(d–f), respectively for the FeCrMnNi HEA and the AISI-348 steel. In the HEA, Xe bubbles are noticeable at 8 dpa, but no further growth is observed at 10 dpa. In addition, as confirmed by the SAED patterns shown as insets in Fig. 6(a) and (c), the FeCrMnNi HEA random solid solution is preserved during and after irradiation confirming that no matrix phase decomposition occurred in this alloy. With respect to the AISI-348 steel, Xe bubbles and displacement damage in the form of black-spots were observed to develop and grew preferentially at the edge of the specimens with increasing dose. RIP was detected to occur at 573 K as indicated by the SAED pattern inset in the BFTEM micrograph in Fig. 6(f). Although the SAED pattern in Fig. 6(f) indicates the presence of amorphous-like rings, this is rather associated with the reduced size nature of precipitates (or even damage clusters/precursors) than to the matrix phase amorphisation (as steels do not easily amorphise) or even self-passivation (although the experiments in the MIAMI-2 facility were carried out in high vacuum of around  $1 \times 10^{-7}$  Pa). Carbonaceous contamination cannot also be discarded.

At higher doses, the FeCrMnNi HEA still has its matrix phase free of precipitation up to 25 dpa as shown in the BFTEM micrograph Fig. 7(a) and the respective SAED pattern inset. The occurrence of RIP was confirmed in the AISI-348 steel also at higher doses shown in the BFTEM micrograph in Fig. 7(b) and the respective SAED pattern inset. With respect to the microstructure of the AISI-348 steel at higher doses, precipitates and black-spots were observed at higher magnifications and they were distinguished by using phase contrast in the TEM as shown in the micrographs in Fig. 7(c) and (d).

#### 3.2.3. 873 K

At higher temperatures such as 873 K, the response of both alloys to

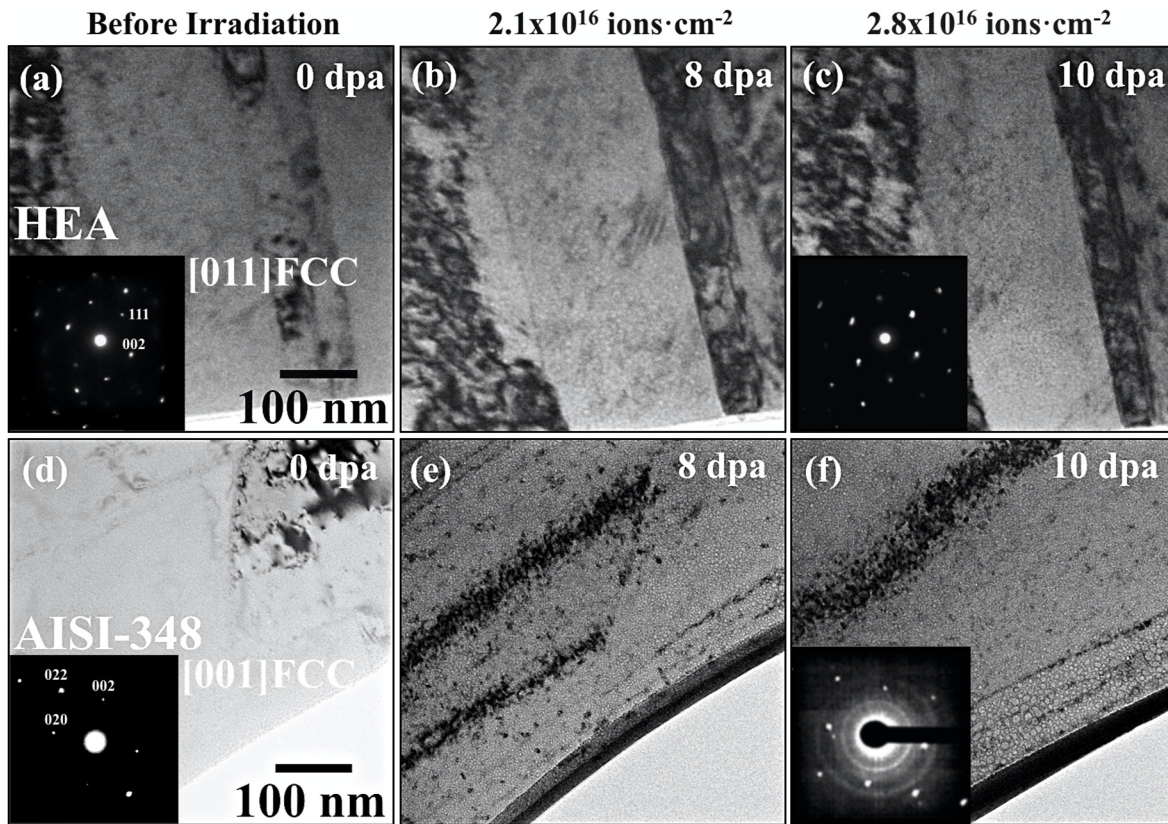


**Fig. 6.** Real-time response of the FeCrMnNi HEA (a–c) and the AISI-348 steel (d–f) upon low-energy heavy ion irradiation up to 10 dpa at 573 K. Note: the scale bar in (a) also applies to (b) and (c) and the scale bar in (d) also applies to (e) and (f).

low-energy heavy ion irradiation was remarkably similar as shown in the micrographs in Fig. 8. Xe bubbles were noticeable in both alloys at a dose of around 2 dpa. Upon increasing the dose, bright areas were observed (under BF conditions) to form and grow. These areas resemble craters or large bubbles, but the occurrence of radiation-induced segregation (RIS) cannot be ruled out. The similarities were also found at higher doses as shown in the BFTEM micrographs in Fig. 9(a–d). Matrix phase decomposition (*i.e.* RIP) was detected in both alloys by the presence of Debye-Scherrer rings in the SAED pattern shown as insets in micrographs 9(a) and 9(c), however, nanometre-sized precipitates were evident in the AISI-348 steel matrix as exhibited in the BFTEM micrograph in Fig. 9(d).

### 3.3. Medium-energy heavy ion irradiation

Medium-energy heavy ion irradiation (300 keV Xe) was used to investigate the response of both alloys at higher doses (around 100 dpa) and the results are shown in this subsection. According to the SRIM calculations, under this irradiation parameters, the number of displacements per ion collision is approximately 1900, thus one order of magnitude higher than the low-energy heavy ion irradiation (30 keV Xe) from the last subsection.

#### 3.3.1. 293 K

The microstructures of the AISI-348 steel and the FeCrMnNi HEA irradiated with 300 keV Xe ions at 293 K up to 123 dpa are shown in the BFTEM micrographs in Fig. 10(a) and (b), respectively, and as demonstrated in the SAED patterns inset within the micrographs, both alloys preserved their matrix phases and RIS or RIP were not observed. Under these irradiation conditions, Xe bubbles were observed to nucleate and grow to larger sizes along the boundaries of Nb(C,N) precipitates as shown in the BFTEM micrograph in Fig. 10(c). In the case of the

FeCrMnNi HEA matrix, a small number of Xe bubbles were observed to grow to larger sizes as shown in the BFTEM micrograph in Fig. 10(d).

#### 3.3.2. 573 K

The results obtained with medium-energy heavy ion irradiation at 573 K diverge from the results at 293 K as shown in the BFTEM micrographs in Fig. 11(a and b). At 140 dpa, both Xe bubbles and black spots were significantly larger in the AISI-348 steel compared with the FeCrMnNi HEA and in addition, the austenite phase was observed to decompose under irradiation in contrast to the HEA as shown in the SAED patterns as insets in Fig. 11(a and b).

## 4. Comprehensive discussion

A summary of the results obtained with low- and medium-energy heavy ion irradiations on both the FeCrMnNi HEA and AISI-348 steel is presented in Table 3 and it is evident that among all the cases analysed in this present research, the FeCrMnNi HEA has a superior radiation tolerance than its ‘‘low-entropy’’ counterpart, the AISI-348 steel. The results are more interesting when the common operational temperature of light-water reactors (LWRs) is taken into consideration, *i.e.* at a temperature of around 573 K; in both irradiation scenarios, the FeCrMnNi HEA matrix phase was stable whereas the AISI-348 steel decomposed into nanometre-sized precipitates.

A comment must be made on the nature of the precipitates formed as a result of heavy ion irradiation in the austenite matrix of the AISI-348 steel. The available literature suggest that the phase is the  $\tau$ -carbide ( $\text{Cr}_{23}\text{C}_6$ ) [70,90,91], although a recent work [92] indicated that due to limited spatial resolution, an overlapping of lattice spacings between different Cr-rich carbide phases ( $\text{Cr}_{23}\text{C}_6$ ,  $\text{M}_6\text{C}$  and MC) will occur in the TEM and by this, a precise characterisation of such precipitates using existing electron microscope methods is not accurate. Due to these

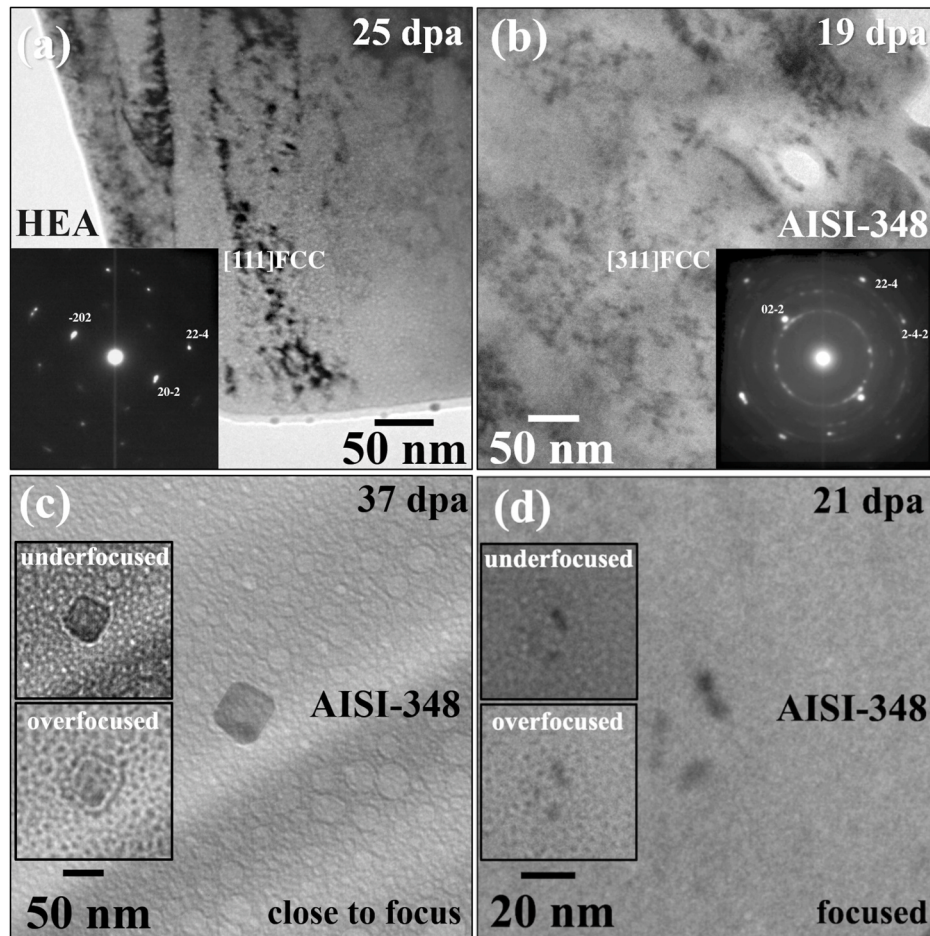


**Fig. 7.** Low-energy heavy ion irradiations at 573 K indicate that even at higher doses (25 dpa), the FeCrMnNi HEA preserves its matrix phase and no RIP/decomposition was detected. On the other hand, Debye-Scherrer rings in the AISI-348 steel indicates the presence of nano-precipitates as shown in micrograph (b). Further analysis using phase contrast in the TEM has shown that the precipitates can be distinguished from black-spots with under and overfocus conditions as shown in micrographs (c) and (d). Note: micrographs (a) and (b) are underfocused to 1000 nm and the defocus in the insets in micrographs (c) and (d) are respectively  $\pm 300$  and  $\pm 1000$  nm.

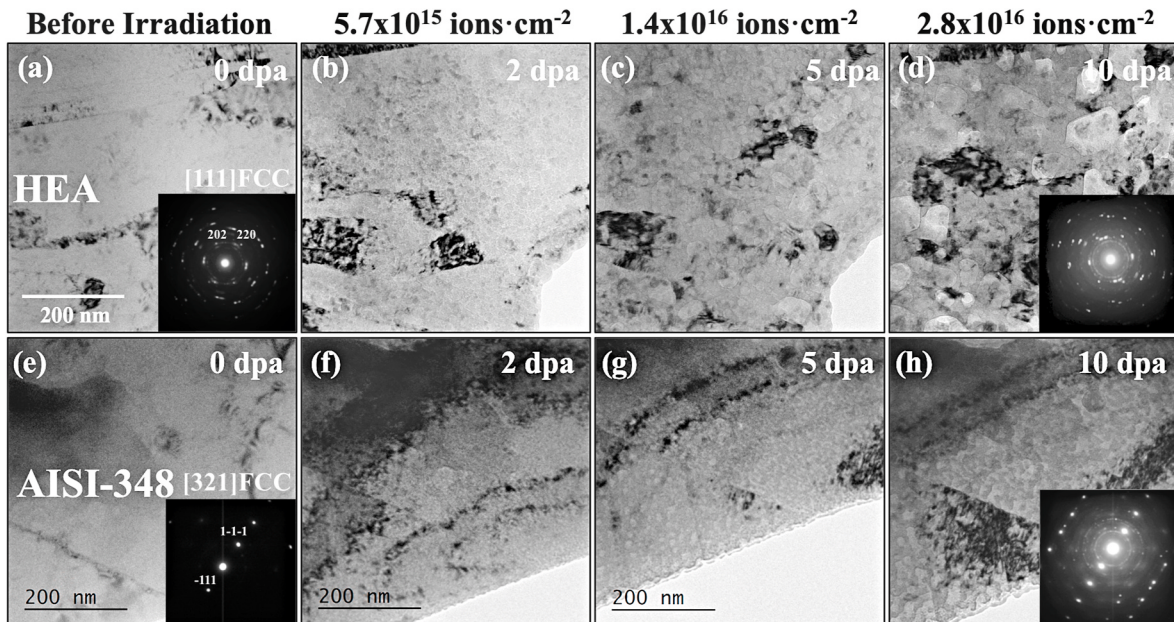


**Fig. 8.** Real-time response of the FeCrMnNi HEA (a-d) and the AISI-348 steel (e-h) upon low-energy heavy ion irradiation up to 10 dpa at 873 K. Note: the scale bar in (a) applies to all micrographs in the figure.

reasons, in this present work, the experimentally observed matrix phase instabilities are confirmed by the presence of Debye-Scherrer rings independent of the crystallographic phase and nature of the formed

precipitates.

The question of whether the HEA constitutive core-effects can be used to shed light on its superior radiation tolerance remains to be

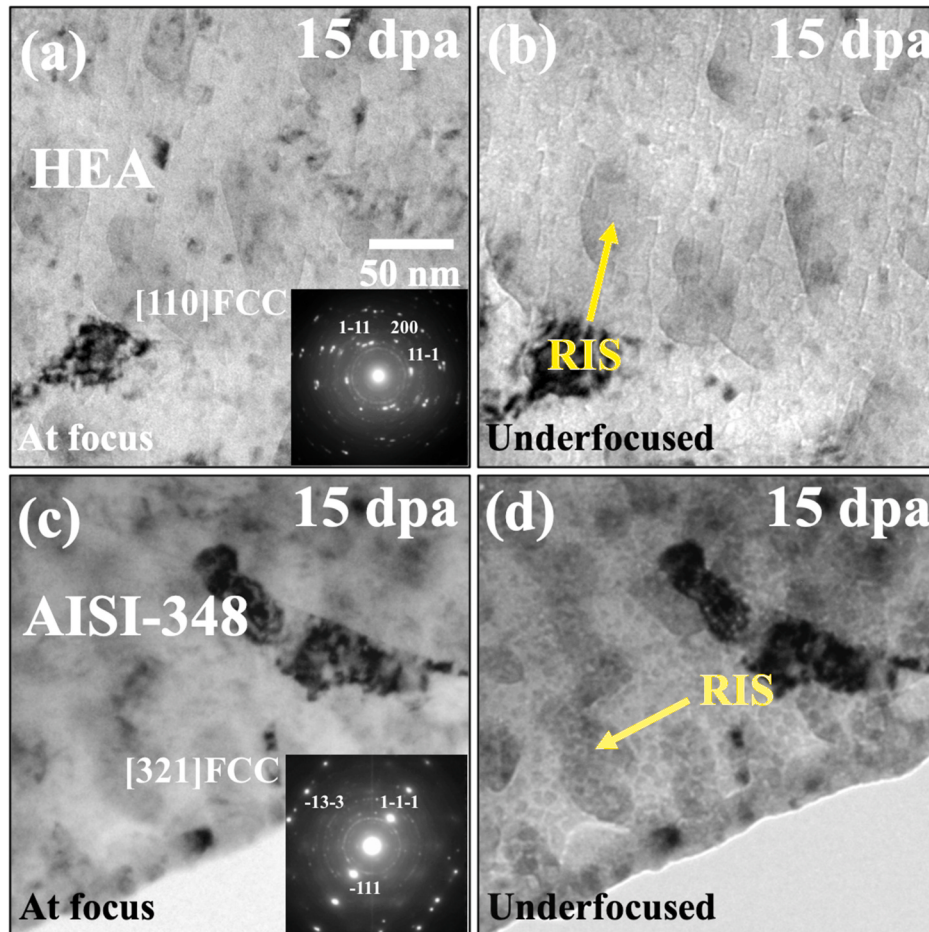


**Fig. 9.** Low-energy heavy ion irradiations at 873 K revealed RIS and RIP in both the FeCrMnNi HEA (a–b) and the AISI-348 steel (c–d). The SAED patterns insets in (a) and (c) also confirm the matrix phase decomposition in both alloys. Note: the scale bar in (a) applies to all micrographs in the figure.

addressed. Firstly, the high thermodynamic phase stability of HEAs is (hypothetically) associated with the high configurational entropy given that the alloy is highly concentrated and (closer to) equiatomic. In fact, equation (1) was used to estimate the configurational entropy for both the FeCrMnNi HEA and the AISI-348 steel and the calculated values are: 11.4 and  $7.4 \text{ J}\cdot\text{K}^{-1}\cdot\text{mol}^{-1}$ , respectively. This simple calculation indicates that the configurational entropy of the FeCrMnNi HEA is around 35% higher than that of the steel.

It is worth emphasising that these calculated values represent the maximum configurational entropy assuming a random solid solution, but as demonstrated by Schön et al. [63–65], these concentrated solid solutions have a certain degree of short range ordering (SRO). Considering SRO levels in HEAs, the configurational entropy is reduced by up to 80–85% of its maximum value in BCC systems. For FCC systems, Schön et al. [93] reported that this reduction is expected to be even higher. SRO becomes less significant in diluted alloys than in concentrated solid solutions, therefore, the entropy reduction in the AISI-348 steel is expected to be smaller than in the FeCrMnNi HEA. This emphasizes that although the calculated entropy difference between the FeCrMnNi HEA and AISI-348 steel is around 35%, the real difference can be smaller. In terms of thermodynamics, this small configurational entropy difference is insufficient to explain the superior matrix phase stability of the FeCrMnNi HEA under extreme irradiation.

The second hypothetical core-effect of HEAs that could play a major role in the observed radiation response of both alloys is the hypothesis of sluggish diffusion. Before discussing, it is worth remembering that a detailed study investigating the sluggish diffusion core-effect in the FeCrMnNi HEA and the AISI-348 steel was carried out by Tunes et al.

[62] who reported that the nucleation and growth of He and Xe inert gas bubbles in both alloys was very similar. If sluggish diffusion existed to suppress the diffusion of point defects (a necessary condition for the nucleation and growth of inert gas bubbles in alloys), the sizes of inert gas bubbles in the AISI-348 steel should be larger than in the FeCrMnNi HEA: the authors observed that within the statistical error, the sizes of bubbles were of similar size in both alloys.

In fact, both impurity and displacement damage types in the form of Xe bubbles and black spots were significantly reduced in the FeCrMnNi HEA compared with the AISI-348 steel. This can be observed, for example, in Fig. 11(a and b). One particular experimental observation made in this present work is that upon increasing the temperature (at 873 K see Fig. 8a–h), the FeCrMnNi HEA was observed to be subjected to RIS/RIP in a similar manner to that in the AISI-348 steel. This suggests that if the HEA core-effects such as sluggish diffusion and high entropy effect do exist, they play a minor role in the radiation response of the FeCrMnNi HEA in the high-temperature regime: this is in disagreement with the high-entropy core-effect, since the thermodynamic stability should increase more at high temperatures. The experimental observations made in this present work agree with recent *ab initio* investigations performed by Zhao et al. [55] who identified that the intrinsic diffusional characteristics of some HEAs (NiFe, NiCo and NiCoCr) diminish at elevated temperatures. Details of the *ab initio* methods used to estimate constitutive parameters of HEAs were recently reviewed by Zhang et al. [45].

Another particular feature of the FeCrMnNi HEA microstructure is the higher density of annealing twins at the nanoscale when compared with the AISI-348 steel. As Zhao et al. [55] commented, in the presence

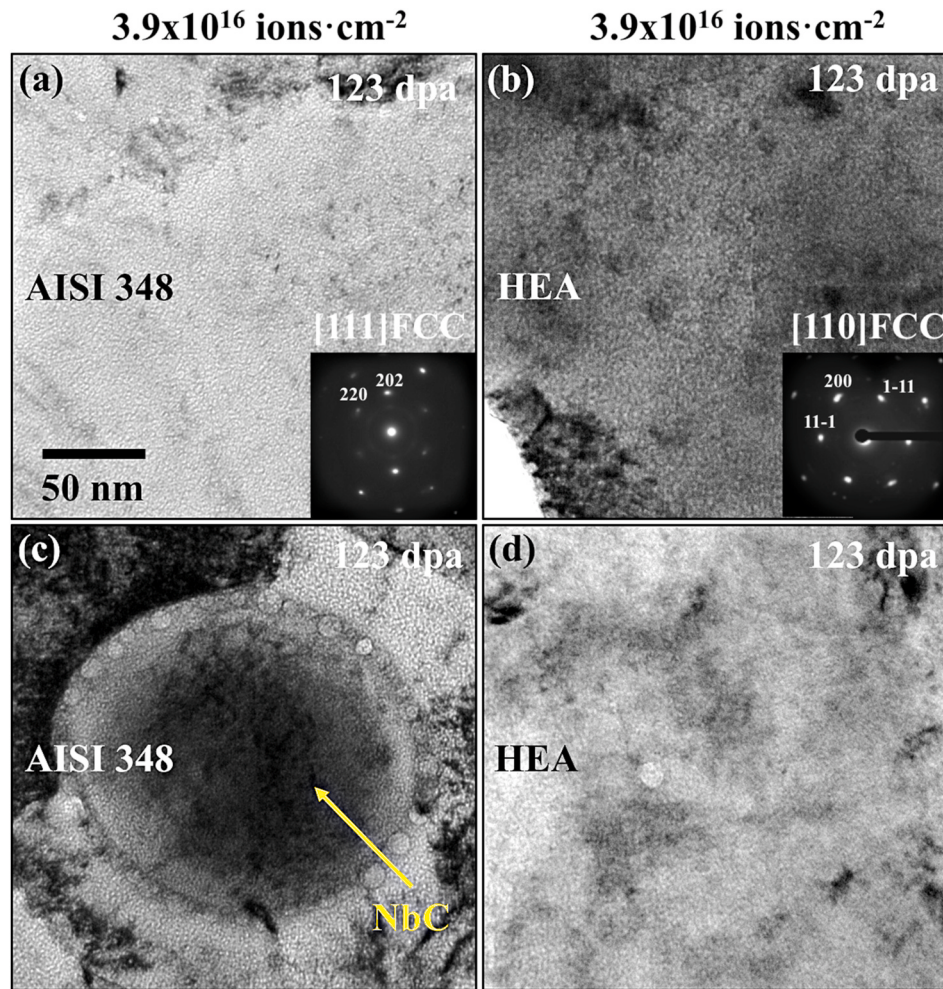


**Fig. 10.** Real-time response of the AISI-348 steel (a–c) and the FeCrMnNi HEA (b–d) upon medium-energy heavy ion irradiation up to 123 dpa at 293 K.

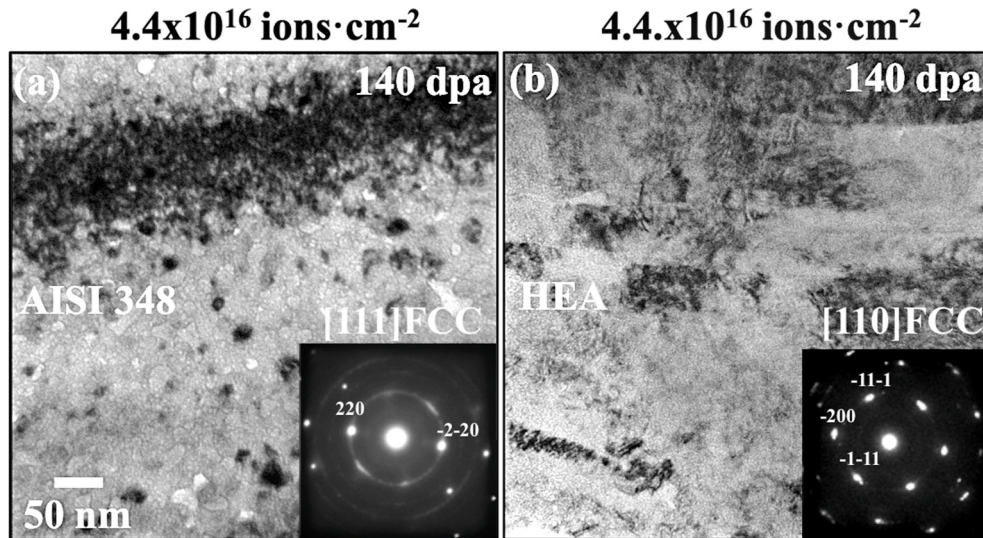


**Fig. 11.** At 573 K and up to 140 dpa medium-energy heavy ion irradiations resulted in RIP in the AISI-348 steel as shown in the BFTEM micrograph (a) and its respective SAED pattern inset whilst the FeCrMnNi HEA preserved its matrix phase as shown in the BFTEM micrograph (b) and its respective SAED pattern inset. Displacement and impurity damage types were also more prone to nucleate and evolve in the steel when compared with the HEA.

of defect sinks, the preferential diffusion of a particular element of the HEA would inevitably lead to RIS and RIP at higher temperatures which explain the results herein observed with the FeCrMnNi HEA irradiated

with 30 keV Xe ions at 873 K. But in the low-temperature regime, the presence of a higher density of annealing twins could serve as preferential sites for radiation-induced diffusive point defects, resulting in

**Table 3**

AISI-348 steel and the FeCrMnNi HEA matrix phase stability under low- and medium-energy heavy ion irradiations in the dose range of 0–140 dpa.

		AISI-348 steel	FeCrMnNi HEA
Low-energy	298 K	Matrix phase decomposed	Matrix phase preserved
	573 K	Matrix phase decomposed	Matrix phase preserved
	873 K	Matrix phase decomposed	Matrix phase decomposed
Medium-energy	298 K	Matrix phase preserved	Matrix phase preserved
	573 K	Matrix phase decomposed	Matrix phase preserved

fewer Xe bubbles as well as black-spots accumulation and growth in the HEA matrix. This later assumption agrees with a previous study by our group [62] where inert gas bubbles were prone to grow along twin boundaries in the FeCrMnNi HEA upon annealing, thus suggesting that these twins are active sink sites of radiation-induced defects. This sheds light that further studies are required to investigate the nature of twinning in this HEA. This can also be the reason for a suppressed susceptibility to RIP in the HEA when compared with the AISI-348 steel, leading to the superior radiation resistance experimentally observed.

## 5. Conclusions

Low- and medium-energy heavy ion irradiations were performed in this work in a FeCrMnNi high-entropy alloy and in the AISI-348 steel as its “low-entropy” counterpart. Within the wide range of irradiation configurations analysed, the FeCrMnNi HEA was more stable to irradiation than the steel in terms of the stability of the matrix phase. A trend for RIP to occur in the AISI-348 steel was observed in almost all the conditions studied.

A surprising metallurgical finding is that by simply tuning the chemical composition, higher radiation tolerance can be achieved in the particular thermodynamic system of Fe–Cr–Mn–Ni. The high configurational entropy and sluggish diffusion core-effects were tested and discussed to reflect on the observed results. Given the low difference between the calculated value of the configurational entropy of the two alloys and the fact that the FeCrMnNi HEA was observed to decompose (as was the steel) in the high-temperature regime, it is unlikely that these core-effects govern the high radiation tolerance observed.

Another observation that must be made on the differences in the radiation response of HEAs and dilute alloys: the observed radiation resistance of the FeCrMnNi HEA indicate that, in general, the HEA will also degrade as the AISI-348 steel does, but such degradation starts at higher temperatures and much higher doses. The presence of internal surfaces in the case of FeCrMnNi HEA – annealing twins – could play a key role on its radiation response, mainly in delaying (on the FeCrMnNi HEA) the observed degradation in the AISI-348 steel, but further research is pending to confirm such a hypothesis.

Although the results indicate that metallic alloying in the highly-concentrated region of phase diagrams result in alloys with superior radiation tolerance, the underlying constitutive hypotheses of this novel metal alloy class require clarification, evidence and, therefore, further research. The role of surfaces as sinks for irradiation-induced defects on both FeCrMnNi HEA and the AISI-348 steel is also another subject for further research investigations. In addition, the nature of the precipitates observed in the FeCrNiMn HEA matrix when subjected to low-energy heavy ion irradiation at 873 K are yet pending of further analytical characterisation.

## CRediT author statement

**MAT:** Conceptualization, Formal Analysis, Investigation and Writing – Original Draft.

**GG:** Conceptualization, Formal Analysis, Investigation and Writing – Review and Editing.

**HB:** Conceptualization, Formal Analysis, Investigation and Writing – Review and Editing.

**PDE:** Conceptualization, Formal Analysis, Investigation, Supervision, Project Funding and Writing – Review and Editing.

**YZ:** Conceptualization, Formal Analysis, Investigation, Supervision, Project Funding and Writing – Review and Editing.

**SED:** Conceptualization, Formal Analysis, Investigation, Supervision, Project Funding and Writing – Review and Editing.

**CGS:** Conceptualization, Formal Analysis, Investigation, Supervision and Writing – Review and Editing.

## Data availability

The raw data required to reproduce these findings are available upon reasonable request.

## Declaration of competing interest

The authors declare that they have no known competing financial interests or personal relationships that could have appeared to influence the work reported in this paper.

## Acknowledgements

All the authors are grateful to the Engineering and Physical Sciences Research Council (EPSRC) of the United Kingdom for funding of MIAMI-2 under grant number EP/M028283/1 and also for funding from the United Kingdom National Ion Beam Centre (UKNIBC) of which the MIAMI facility is a part. MAT is grateful for a previous funding through the ASTRO fellowship, a United States Department of Energy workforce development program implemented at Oak Ridge National Laboratory through the Oak Ridge Institute for Science and Education under Contract DE-AC05-06OR23100. CGS acknowledges the financial support from the Brazilian National Research, Technology and Innovation Council (CNPq) under grant 308565/2018-5. YZ and HB were supported as part of the Energy Dissipation to Defect Evolution (EDDE), an Energy Frontier Research Centre funded by the U.S. Department of Energy, Office of Science, Basic Energy Sciences under contract number DE-AC05-00OR22725. MAT would like to thank Professor Frank A. Garner (DSL Extreme and Texas A&M University) for assessing this paper and for many discussions on austenitic steels in extreme environments. MAT would like to thank Professor Steve G. Roberts (University of Oxford) and Professor Konstantina Lambrinou (University of Huddersfield) for an accurate evaluation of his PhD thesis [81] including many valuable suggestions provided during examination which has improved the final revised version of the thesis.

## References

- [1] L. Stemper, B. Mitas, T. Kremmer, S. Otterbach, P.J. Uggowitzer, S. Pogatscher, Age-hardening of high pressure die casting AlMg alloys with Zn and combined Zn and Cu additions, Mater. Des. 181 (2019), 107927.
- [2] L. Stemper, M.A. Tunes, P. Oberhauser, P.J. Uggowitzer, S. Pogatscher, Age-hardening response of AlMgZn alloys with Cu and Ag additions, Acta Mater. 195 (2020) 541–554.
- [3] T.M. Kremmer, P. Dumitraschkevitz, D. Pöschmann, T. Ebner, P.J. Uggowitzer, G. K. Kolb, S. Pogatscher, Microstructural change during the interrupted quenching of the AlZnMg (Cu) alloy AA7050, Materials 13 (11) (2020) 2554.
- [4] J. Grasserbauer, I. Weissensteiner, G. Falkinger, S. Mitsche, P.J. Uggowitzer, S. Pogatscher, Evolution of microstructure and texture in laboratory-and industrial-scaled production of automotive Al-sheets, Materials 13 (2) (2020) 469.
- [5] P. Dumitraschkevitz, P.J. Uggowitzer, S.S. Gerstl, J.F. Löffler, S. Pogatscher, Size-dependent diffusion controls natural aging in aluminium alloys, Nat. Commun. 10 (1) (2019) 1–6.
- [6] B. Gruber, F. Grabner, G. Falkinger, A. Schökel, F. Spieckermann, P.J. Uggowitzer, S. Pogatscher, Room Temperature Recovery of Cryogenically Deformed Aluminium Alloys, Materials & Design, 2020, 108819.

- [7] F. Schmid, P.J. Uggowitzer, R. Schäublin, M. Werinos, T. Ebner, S. Pogatscher, Effect of thermal treatments on Sn-Alloyed Al-Mg-Si alloys, *Materials* 12 (11) (2019) 1801.
- [8] J.A. Österreicher, M. Kumar, A. Schiffel, S. Schwarz, D. Hillebrand, G.R. Bourret, Sample preparation methods for scanning electron microscopy of homogenized Al-Mg-Si billets: a comparative study, *Mater. Char.* 122 (2016) 63–69.
- [9] J.A. Österreicher, G. Kirov, S.S. Gerstl, E. Mukeli, F. Grabner, M. Kumar, Stabilization of 7xxx aluminium alloys, *J. Alloys Compd.* 740 (2018) 167–173.
- [10] J.A. Österreicher, C. Simson, A. Großalber, S. Frank, S. Gneiger, Spatial lithium quantification by backscattered electron microscopy coupled with energy-dispersive x-ray spectroscopy, *Scripta Mater.* 194 (2021), 113664.
- [11] A.C. Hänzi, I. Gerber, M. Schinhammer, J.F. Löffler, P.J. Uggowitzer, On the in vitro and in vivo degradation performance and biological response of new biodegradable Mg-Y-Zn alloys, *Acta Biomater.* 6 (5) (2010) 1824–1833.
- [12] Y.-Q. Jiang, Y. Lin, X.-Y. Jiang, D.-G. He, X.-Y. Zhang, N. Kotkunde, Hot tensile properties, microstructure evolution and fracture mechanisms of Ti-6Al-4V alloy with initial coarse equiaxed phases, *Mater. Char.* (2020) 110272.
- [13] N.P. Papenberg, S. Gneiger, I. Weißensteiner, P.J. Uggowitzer, S. Pogatscher, Mg-alloys for forging applications—a review, *Materials* 13 (4) (2020) 985.
- [14] H. Bhadeshia, R. Honeycombe, Steels: Microstructure and Properties, Butterworth-Heinemann, 2017.
- [15] L. Scheer, Was ist Stahl: eine Stahlkunde für jedermann, Springer-Verlag, 2013.
- [16] H. Rickover, L. Geiger, B. Lustman, History of the Development of Zirconium Alloys for Use in Nuclear Reactors, Tech. Rep., Energy Research and Development Administration, Washington, D.C. (USA), 1975. Div. of Naval Reactors, Washington, DC.
- [17] M.T. Simnad, A brief history of power reactor fuels, *J. Nucl. Mater.* 100 (1–3) (1981) 93–107.
- [18] S. Zinkle, G. Was, Materials challenges in nuclear energy, *Acta Mater.* 61 (3) (2013) 735–758.
- [19] Y. Zhang, T. Egami, W.J. Weber, Dissipation of radiation energy in concentrated solid-solution alloys: unique defect properties and microstructural evolution, *MRS Bull.* 44 (10) (2019) 798–811.
- [20] E.R. Eaton, H. McKerrel, Near eastern alloying and some textual evidence for the use of arsenical copper, *World Archeol.* 8 (1976) 169–191.
- [21] M. Radivojević, T. Rehren, J. Kuzmanović-Cvetović, M. Jovanović, J. P. Northover, Tainted ores and the rise of tin Bronzes in Eurasia, *Antiquity* 87 (2013) 1030–1045.
- [22] T. Rose, P. Télouk, S. Klein, H.R. Marschall, Questioning Fe isotopes as a provenance tool: insights from bog iron ores and alternative applications in archeometry, *J. Archeol. Sci.* 101 (2019) 52–62.
- [23] W. Hume-Rothery, R.E. Smallman, C.W. Haworth, The Structure of Metals and Alloys, The Institute of Metals, 1969.
- [24] D.A. Porter, K.E. Easterling, M. Sherif, Phase Transformations in Metals and Alloys, CRC press, 2009.
- [25] B. Murty, J.-W. Yeh, S. Ranganathan, High-entropy Alloys, Butterworth-Heinemann, 2014.
- [26] F.C. Achard, Recherches sur les propriétés des alliages métalliques, Imprimé chez George Jacques Decker & Fils, 1788.
- [27] B. Cantor, K. Kim, P.J. Warren, Novel Multicomponent Amorphous Alloys, in: Materials Science Forum, vol. 386, Trans Tech Publ, 2002, pp. 27–32.
- [28] B. Cantor, I. Chang, P. Knight, A. Vincent, Microstructural development in equiatomic multicomponent alloys, *Mater. Sci. Eng.* 375 (2004) 213–218.
- [29] B. Cantor, Stable and metastable multicomponent alloys, *Ann. Chem.* 32–3 (2007) 245–256. Lavoisier.
- [30] B. Cantor, Multicomponent and high entropy alloys, *Entropy* 16 (9) (2014) 4749–4768.
- [31] J.W. Yeh, Y.L. Chen, S.J. Lin, S.K. Chen, High-entropy Alloys—A New Era of Exploitation, in: Materials Science Forum, vol. 560, Trans Tech Publ, 2007, pp. 1–9.
- [32] J.-W. Yeh, Alloy design strategies and future trends in high-entropy alloys, *JOM* 65 (12) (2013) 1759–1771.
- [33] J.-W. Yeh, Physical metallurgy of high-entropy alloys, *JOM* 67 (10) (2015) 2254–2261.
- [34] X. Yan, Y. Zhang, Functional properties and promising applications of high entropy alloys, *Scripta Mater.* 187 (2020) 188–193.
- [35] K. Sharp, F. Matschinsky, Translation of Ludwig Boltzmann's paper "On the relationship between the second fundamental theorem of the mechanical theory of heat and probability calculations regarding the conditions for thermal equilibrium" *sitzungsberichte der kaiserlichen akademie der wissenschaften. mathematisch-naturwissen classe. abt. ii, lxxvi 1877, pp 373-435 (wien. ber. 1877, 76: 373-435).* reprinted in *wiss. abhandlungen, vol. ii, reprint 42, p. 164-223, Barth, Leipzig, 1909, Entropy* 17 (4) (2015) 1971–2009.
- [36] B. Fultz, Vibrational thermodynamics of materials, *Prog. Mater. Sci.* 55 (4) (2010) 247–352.
- [37] R.A. Swalin, J. Arents, Thermodynamics of solids, *J. Electrochem. Soc.* 109 (12) (1962) 308C, 308C.
- [38] Y. Jien-Wei, Recent progress in high entropy alloys, *Ann. Chimie Sci. Matériaux* 31 (6) (2006) 633–648.
- [39] K.-H. Cheng, C.-H. Lai, S.-J. Lin, J.-W. Yeh, Structural and mechanical properties of multi-element (AlCrMoTaTiZr)<sub>n<sub>x</sub></sub> coatings by reactive magnetron sputtering, *Thin Solid Films* 519 (10) (2011) 3185–3190.
- [40] M.-H. Tsai, J.-W. Yeh, J.-Y. Gan, Diffusion barrier properties of almonbsitativzr high-entropy alloy layer between copper and silicon, *Thin Solid Films* 516 (16) (2008) 5527–5530.
- [41] K.-Y. Tsai, M.-H. Tsai, J.-W. Yeh, Reply to comments on "Sluggish diffusion in Co-Cr-Fe-Mn-Ni high-entropy alloys", in: K.Y. Tsai, M.H. Tsai, J.W. Yeh (Eds.), *Acta Mater.* 61 (2013) 4887–4897. *Scripta Materialia* 135 (2017) 158–159.
- [42] A. Paul, Comments on "Sluggish diffusion in Co-Cr-Fe-Mn-Ni high-entropy alloys", in: K.Y. Tsai, M.H. Tsai, J.W. Yeh (Eds.), *Acta Mater.* 61 (2013) 4887–4897. *Scripta Materialia* 135 (2017) 153–157.
- [43] K.-Y. Tsai, M.-H. Tsai, J.-W. Yeh, Sluggish diffusion in co-cr-fe-mn-ni high-entropy alloys, *Acta Mater.* 61 (13) (2013) 4887–4897.
- [44] C. Li, X. Hu, T. Yang, N.K. Kumar, B.D. Wirth, S.J. Zinkle, Neutron irradiation response of a Co-free high entropy alloy, *J. Nucl. Mater.* 527 (2019), 151838.
- [45] Y. Zhang, S. Zhao, W.J. Weber, K. Nordlund, F. Granberg, F. Djurabekova, Atomic-level heterogeneity and defect dynamics in concentrated solid-solution alloys, *Curr. Opin. Solid State Mater. Sci.* 21 (5) (2017) 221–237.
- [46] Y. Zhang, M.A. Tunes, M.L. Crespiello, F. Zhang, W.L. Boldman, P.D. Rack, L. Jiang, C. Xu, G. Greaves, S.E. Donnelly, L. Wang, W.J. Weber, Thermal stability and irradiation response of nanocrystalline CoCrCuFeNi high-entropy alloy, *Nanotechnology* 30 (29) (2019), 294004.
- [47] M.A. Tunes, V.M. Vishnyakov, O. Camara, G. Greaves, P.D. Edmondson, Y. Zhang, S.E. Donnelly, A candidate accident tolerant fuel system based on a highly concentrated alloy thin film, *Mater. Today Energy* 12 (2019) 356–362.
- [48] Y. Zhang, G.M. Stocks, K. Jin, C. Lu, H. Bei, B.C. Sales, L. Wang, L.K. Béland, R. E. Stoller, G.D. Samolyuk, et al., Influence of chemical disorder on energy dissipation and defect evolution in concentrated solid solution alloys, *Nat. Commun.* 6 (2015) 8736.
- [49] N.A.P.K. Kumar, K.J. Leonard, H. Bei, T.S. Byun, Y. Zhang, S.J. Zinkle, H.B.K. J. Leonard, T.S. Byun, Y. Zhang, S.J. Zinkle, Ion Irradiation effects on high-entropy alloy, *Fusion React. Mater. Progr.* 54 (2013) 145–153.
- [50] N.K. Kumar, C. Li, K. Leonard, H. Bei, S. Zinkle, Microstructural stability and mechanical behavior of FeNiMnCr high entropy alloy under ion irradiation, *Acta Mater.* 113 (2016) 230–244.
- [51] C. Lu, L. Niu, N. Chen, K. Jin, T. Yang, P. Xiu, Y. Zhang, F. Gao, H. Bei, S. Shi, M.-R. He, I.M. Robertson, W.J. Weber, L. Wang, Enhancing radiation tolerance by controlling defect mobility and migration pathways in multicomponent single-phase alloys, *Nat. Commun.* 7 (2016), 13564.
- [52] C. Lu, T. Yang, K. Jin, N. Gao, P. Xiu, Y. Zhang, F. Gao, H. Bei, W.J. Weber, K. Sun, et al., Radiation-induced segregation on defect clusters in single-phase concentrated solid-solution alloys, *Acta Mater.* 127 (2017) 98–107.
- [53] R. Harrison, G. Greaves, H. Le, H. Bei, Y. Zhang, S. Donnelly, Chemical effects on he bubble superlattice formation in high entropy alloys, *Curr. Opin. Solid State Mater. Sci.* 23 (4) (2019), 100762.
- [54] S. Zhao, W.J. Weber, Y. Zhang, Unique challenges for modeling defect dynamics in concentrated solid-solution alloys, *JOM* 69 (11) (2017) 2084–2091.
- [55] S. Zhao, Y. Ossetsky, Y. Zhang, Preferential diffusion in concentrated solid solution alloys: NiFe, NiCo and NiCoCr, *Acta Mater.* 128 (2017) 391–399.
- [56] H.K.D.H. Bhadeshia, High entropy alloys, *Mater. Sci. Technol.* 31 (10) (2015) 1139–1141.
- [57] R.B. McLellan, W.W. Dunn, A quasi-chemical treatment of interstitial solid solutions: its application to carbon austenite, *J. Phys. Chem. Solid.* 30 (11) (1969) 2631–2637.
- [58] W.W. Dunn, R.B. McLellan, The application of a quasichemical solid solution model to carbon austenite, *Metall. Mater. Trans. B* 1 (5) (1970) 1263–1265.
- [59] S. Ma, J. Xing, D. Yi, H. Fu, J. Zhang, Y. Li, Z. Zhang, G. Liu, B. Zhu, Effects of chromium addition on corrosion resistance of fe-3.5 b alloy in liquid zinc, *Surf. Coatings. Technol.* 205 (21–22) (2011) 4902–4909.
- [60] R. Mishra, N. Kumar, M. Komarasamy, Lattice strain framework for plastic deformation in complex concentrated alloys including high entropy alloys, *Mater. Sci. Technol.* 31 (10) (2015) 1259–1263.
- [61] J. Dabrowska, M. Zajusz, W. Kucza, G. Cieslak, K. Berent, T. Czepe, T. Kulik, M. Danielewski, Demystifying the sluggish diffusion effect in high entropy alloys, *J. Alloys Compd.* 783 (2019) 193–207.
- [62] M.A. Tunes, H. Le, G. Greaves, C.G. Schön, H. Bei, Y. Zhang, P.D. Edmondson, S. E. Donnelly, Investigating sluggish diffusion in a concentrated solid solution alloy using ion irradiation with in situ TEM, *Intermetallics* 110 (2019), 106461.
- [63] C.G. Schön, M.A. Tunes, R. Arróyave, J. Ågren, On the complexity of solid-state diffusion in highly concentrated alloys and the sluggish diffusion core-effect, *Calphad* 68 (2020), 101713.
- [64] C.G. Schön, T. Duong, Y. Wang, R. Arróyave, Probing the entropy hypothesis in highly concentrated alloys, *Acta Mater.* 148 (2018) 263–279.
- [65] C.G. Schön, T. Duong, Y. Wang, R. Arróyave, A proof of concept: thermodynamics of aluminum-transition metal highly concentrated alloys, *J. Alloys Compd.* 781 (2019) 595–605.
- [66] F. Tuomisto, I. Makkonen, J. Heikinheimo, F. Granberg, F. Djurabekova, K. Nordlund, G. Velisa, H. Bei, H. Xue, W. Weber, et al., Segregation of Ni at early stages of radiation damage in NiCoFeCr solid solution alloys, *Acta Mater.* 196 (2020) 44–51.
- [67] A. Padilha, R. Plaut, P. Rios, Stainless Steels Heat Treatment (Chapter 12), Steel Heat Treatment, CRC Press, Boca Raton, 2007.
- [68] Fopil, Solutions in stainless steels (jun 2020). <https://fopil.com.br/solucoes-em-aco-inox/>, 2020.
- [69] L.A. Giannuzzi, et al., Introduction to Focused Ion Beams: Instrumentation, Theory, Techniques and Practice, Springer Science & Business Media, 2004.
- [70] M.A. Tunes, G. Greaves, T.M. Kremmer, V.M. Vishnyakov, P.D. Edmondson, S. E. Donnelly, S. Pogatscher, C.G. Schön, Thermodynamics of an austenitic stainless steel (AISI-348) under in situ TEM heavy ion irradiation, *Acta Mater.* 179 (2019) 360–371.

- [71] B. Fultz, J.M. Howe, *Transmission Electron Microscopy and Diffractometry of Materials*, Springer Science & Business Media, 2012.
- [72] C. Rarey, J. Stringer, J. Edington, Crystallographic techniques for the interpretation of transmission electron micrographs of hexagonal metals, *Trans. A. I.M.E.* 236 (5) (1966) 811–812.
- [73] A. Oila, S. Bull, Atomistic simulation of fe–c austenite, *Comput. Mater. Sci.* 45 (2) (2009) 235–239.
- [74] G. Greaves, A. Mir, R. Harrison, M. Tunes, S. Donnelly, J. Hinks, New microscope and ion accelerators for materials investigations (MIAMI-2) system at the University of Huddersfield, *Nucl. Instrum. Methods Phys. Res. Sect. A Accel. Spectrom. Detect. Assoc. Equip.* 931 (2019) 37–43.
- [75] J.F. Ziegler, M.D. Ziegler, J.P. Biersack, Srim—the stopping and range of ions in matter, *Nucl. Instrum. Methods Phys. Res. Sect. B Beam Interact. Mater. Atoms* 268 (11–12) (2010) 1818–1823, 2010.
- [76] R.E. Stoller, M.B. Toloczko, G.S. Was, A.G. Certain, S. Dwarakanath, F.A. Garner, On the use of srim for computing radiation damage exposure, *Nucl. Instrum. Methods Phys. Res. Sect. B Beam Interact. Mater. Atoms* 310 (2013) 75–80.
- [77] W.J. Weber, Y. Zhang, Predicting damage production in monoatomic and multi-elemental targets using stopping and range of ions in matter code: challenges and recommendations, *Curr. Opin. Solid State Mater. Sci.* 23 (4) (2019), 100757.
- [78] K.K. Chawla, M. Meyers, *Mechanical Behavior of Materials*, Prentice Hall Upper, Saddle River, 1999.
- [79] J.M. Silcock, W.J. Tunstall, Partial dislocations associated with NbC precipitation in austenitic stainless steels, *Phil. Mag.* 10 (105) (1964) 361–389.
- [80] M.G.D.V. Cuppari, S.F. Santos, Physical properties of the NbC carbide, *Metals* 6 (10) (2016) 250.
- [81] M.A. Tunes, A Transmission Electron Microscopy Study of Radiation Damage in Potential Nuclear Materials, PhD. thesis, University of Huddersfield, 2020.
- [82] N. Terao, B. Sasamal, Precipitation of m23c6 type carbide on twin boundaries in austenitic stainless steels, *Metallography* 13 (2) (1980) 117–133.
- [83] E. Lee, T. Byun, J. Hunn, M. Yoo, K. Farrell, L. Mansur, On the origin of deformation microstructures in austenitic stainless steel: part i—microstructures, *Acta Mater.* 49 (16) (2001) 3269–3276.
- [84] E. Lee, M. Yoo, T. Byun, J. Hunn, K. Farrell, L. Mansur, On the origin of deformation microstructures in austenitic stainless steel: Part ii—mechanisms, *Acta Mater.* 49 (16) (2001) 3277–3287.
- [85] V. Tsakiris, D. Edmonds, Martensite and deformation twinning in austenitic steels, *Mater. Sci. Eng.* 273 (1999) 430–436.
- [86] Y. Shen, X. Li, X. Sun, Y. Wang, L. Zuo, Twinning and martensite in a 304 austenitic stainless steel, *Mater. Sci. Eng.* 552 (2012) 514–522.
- [87] J. Lu, L. Hultman, E. Holmström, K.H. Antonsson, M. Grehk, W. Li, L. Vitos, A. Golpayegani, Stacking fault energies in austenitic stainless steels, *Acta Mater.* 111 (2016) 39–46.
- [88] C.A. English, B.L. Eyre, Heavy-ion damage in alpha-Fe, *Nature* 260 (1976) 619–621.
- [89] R. Odette, S. Zinkle, *Structural Alloys for Nuclear Energy Applications*, Elsevier, 2019.
- [90] S. Jin, L. Guo, F. Luo, Z. Yao, S. Ma, R. Tang, Ion irradiation-induced precipitation of Cr<sup>23</sup>C<sub>6</sub> at dislocation loops in austenitic steel, *Scripta Mater.* 68 (2) (2013) 138–141.
- [91] M.A. Tunes, C.G. Schön, G. Greaves, Radiation-induced precipitation with concurrent bubbles formation in an austenitic stainless steel (aisi-348), *Materialia* 7 (2019), 100408.
- [92] Í.M. Oyarzabal, M.A. Tunes, O. Camara, E. Aradi, A.H. Mir, G. Greaves, J.A. Hinks, P.F. Fitchner, S.E. Donnelly, The effect of flux on ion irradiation-enhanced precipitation in AISI-316L: an in-situ TEM study, *J. Nucl. Mater.* (2020) 152414.
- [93] C.G. Schön, G. Inden, CVM study of FCC and BCC Ising magnets with generalised spin number, *J. Magn. Magn Mater.* 232 (3) (2001) 209–220.